

# COMPUTATIONAL STUDIES OF ANISOTROPIC DIFFUSE INTERFACE MODEL OF MICROSTRUCTURE FORMATION IN SOLIDIFICATION

MICHAL BENEŠ

**ABSTRACT.** The growth of microstructure non-convex patterns is studied by means of the modified anisotropic phase-field model. The numerical algorithm is designed using the finite-difference spatial discretisation in the method of lines. Results of numerical analysis of the model are based on the a-priori estimates, the compactness and monotonicity arguments. As a quantitative result, we present the convergence studies of the dendritic growth when the mesh size and the diffuse parameter tend to zero.

## 1. INTRODUCTION

The aim of the article is to present numerical convergence of non-convex patterns for the system of phase-field equations endowed by anisotropy. The equations represent a mathematical model of solidification of pure crystalline substances at microscale.

The mentioned physical phenomenon is accompanied by presence of an interface between phases which can move in space and is determined intrinsically by the state of the physical system, its boundary and initial data.

Among various approaches to the mathematical treatment of the problem (e.g. see [22]), the diffuse-interface model yields a well controlled smooth approximation of the characteristic function of phase as a part of the solution. This fact originally observed in the form of a wave-like solution of reaction-diffusion systems (see [1],

---

Received November 20, 2005.

2000 *Mathematics Subject Classification.* Primary 80A22, 82C26, 35A40.

*Key words and phrases.* Phase-field method, finite-difference method, monotonicity method, dendritic growth.

[21]) leads to the formulation of a model of solidification with additional consequences in understanding physics of phase transitions ([19], [20]).

The model equations consist of the heat equation with nearly singular heat source coupled to a semilinear or quasilinear parabolic equation for the order parameter known as the Allen-Cahn equation or equation of phase. The equations in various setting were studied in, e.g. [13], [14], and applied in simulation of physical phenomena ([23], [2], [7]).

The application of models based on the phase-field theory rose several quantitative questions concerning relation to the sharp-interface analogue ([7]). Problems of choice of the small parameter versus mesh size, and problems with interface stability lead to various modifications mainly in the Allen-Cahn equation (see [12], [15], [3], [5]).

Quantitative comparison, performed especially in case of curve motion (or hypersurface motion) driven by mean curvature (see [11]) showed a satisfactory agreement of numerical computations with the analytical solution (where it was possible) or with results obtained by numerical solution of other models, and rised a question about how the anisotropy can be incorporated into the Allen-Cahn equation without losing a possibility of weak formulation which requires a second-order space differential operator in the divergence form (see [4]). This has been done e.g. in [8] for the case of mean-curvature flow, and in [4] for the full phase-field model. The viscosity solution concept allowed to treat even a fully anisotropic (i.e. the case when the kinetic term is also direction-dependent) Allen-Cahn equation not coupled to the heat equation – [16].

The paper extends the scope of [4], where the anisotropic model has been presented in the following form:

$$(1.1) \quad \begin{aligned} \frac{\partial u}{\partial t} &= \nabla^2 u + L\chi'(p) \frac{\partial p}{\partial t}, \\ \xi \frac{\partial p}{\partial t} &= \xi \nabla \cdot T^0(\nabla p) + \frac{1}{\xi} f_0(p) + F(u)\xi\Phi^0(\nabla p), \end{aligned}$$

with initial conditions

$$u|_{t=0} = u_0, \quad p|_{t=0} = p_0,$$

and with boundary conditions of Dirichlet type

$$u|_{\partial\Omega} = 0, \quad p|_{\partial\Omega} = 0,$$

for simplicity. Here,  $\xi > 0$  is the “small” parameter (thickness of the interface), and  $f_0$  the derivative of double-well potential. The coupling function  $F(u)$  is bounded and continuous, or even Lipschitz-continuous. The anisotropy is included using the monotone operator  $T^0$  converting the gradient (see below).

We consider  $f_0(p) = ap(1-p)(p - \frac{1}{2})$  with  $a > 0$ . The enthalpy is given by  $\mathcal{H}(u) = u - L\chi(p)$ , where the coupling function  $\chi$  is monotone with bounded, Lipschitz-continuous derivative:  $\chi(0) = 0$ ,  $\chi(0.5) = 0.5$ ,  $\chi(1) = 1$ ,  $\text{supp}(\chi') \subset \langle 0, 1 \rangle$ . For the sake of simplicity,  $\Omega$  is rectangle. Obviously, the extension to higher dimensions, and to other boundary conditions is possible. Similarly, the forcing term  $F(u)\xi\Phi^0(\nabla p)$  can be modified into  $F(u)\xi\tilde{\Phi}^0(\nabla p)$  where  $\tilde{\Phi}^0$  is another anisotropy – see [10].

The analysis presented in this article has been motivated by numerical studies obtained by the model both for the case of curve dynamics in the plane (see [8], and [10]), and for the case of microstructure growth in solidification (see [4]). The model works with an anisotropy rigorously implemented into the equations. Finally, the model gives reasonable results even in case of non-convex anisotropies, when the mentioned theory is not applied. Our aim is to present numerical convergence results for the onset of dendritic growth.

## 2. MATHEMATICAL ASPECTS OF THE MODEL

The anisotropy is incorporated into the phase-field model according to the approach developed by the author in [4] and [8], which also is influenced by the literature cited therein. Main idea is in replacing isotropic Euclidean norm in  $\mathbb{R}^2$  by another norm exhibiting the desired anisotropy, and in replacing derivatives in a corresponding way.

For this purpose, we introduce a nonnegative function  $\Phi^0 : \mathbb{R}^2 \rightarrow \mathbb{R}_0^+$  which is smooth, strictly convex,  $\mathcal{C}^2(\mathbb{R}^n \setminus \{0\})$  and satisfies:

$$(2.1) \quad \Phi^0(t\eta) = |t|\Phi^0(\eta), \quad t \in \mathbb{R}, \quad \eta \in \mathbb{R}^2,$$

$$(2.2) \quad \lambda|\eta| \leq \Phi^0(\eta) \leq \Lambda|\eta|,$$

where  $\lambda, \Lambda > 0$ . The function satisfies the following relation

$$\Phi^0(\eta) = \Phi_\eta^0(\eta) \cdot \eta, \quad \eta \in \mathbb{R}^2,$$

where the index  $\eta$  denotes derivative of  $\Phi^0$  (i.e.,  $\Phi_\eta^0 = (\partial_{\eta_1} \Phi^0, \partial_{\eta_2} \Phi^0)$ ). We define the map  $T^0 : \mathbb{R}^2 \rightarrow \mathbb{R}^2$  as

$$T^0(\eta) := \Phi^0(\eta)\Phi_\eta^0(\eta) \quad \text{for } \eta \neq 0,$$

$$T^0(0) := 0.$$

The  $\Phi^0$ -normal vector (the Cahn-Hoffmann vector – see [24]) and velocity of a level set

$$\Gamma(t) = \{x \in \mathbb{R}^2 \mid P(t, x) = \text{const.}\},$$

given by a suitable field  $P$  depending on time and space are

$$\mathbf{n}_{\Gamma, \Phi} = -\frac{T^0(\nabla P)}{\Phi^0(\nabla P)}, \quad v_{\Gamma, \Phi} = \frac{\partial_t P}{\Phi^0(\nabla P)}.$$

The anisotropic curvature is given by the formula

$$\kappa_{\Gamma, \Phi} = \text{div}(\mathbf{n}_{\Gamma, \Phi}).$$

In [8], the law

$$v_{\Gamma, \Phi} = -\kappa_{\Gamma, \Phi} + F,$$

has been studied by the phase-field method, in particular by the Allen-Cahn equation as in (1.1).

**Example.** In case of  $\mathbb{R}^2$ , we may use the polar coordinates of a vector  $\eta \in \mathbb{R}^2$  denoted by  $\varrho$  and  $\theta$  to define

$$\Phi^0(\eta) = \varrho f(\theta),$$

for a suitable  $2\pi$ -periodic function  $f$  (we choose  $f(\theta) = 1 + A \cos(m(\theta - \theta_0))$  where  $A$  is the anisotropy strength and  $m \in \mathbb{N}_0$  the anisotropy type).  $\Phi^0$  therefore belongs to  $\mathcal{C}^1(\mathbb{R}^2)$  and  $\mathcal{C}^2(\mathbb{R}^2 \setminus \{0\})$  provided  $\Psi$  belongs to  $\mathcal{C}^2(\langle 0, 2\pi \rangle_{\text{per}})$ . Figure 2.1 depicts the Frank diagram for an example of  $f$  – see [17] for definitions. Note that in case of  $m$  being odd, the rule (2.1) does not hold, but  $\Phi^0$  still can be used in the model.

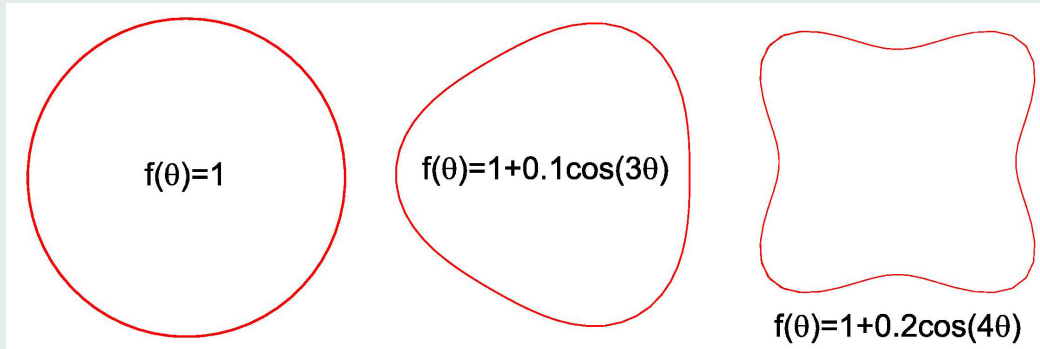


**Figure 2.1.** The Frank diagram of anisotropy.

The above given setting allows to study the model (1.1) by the monotonicity and compactness methods. We denote:

$$(u, v) = \int_{\Omega} uv \, dx \quad \text{for } u, v \in L_2(\Omega),$$

the usual  $L_2$ -scalar product. We define the weak solution of (1.1) as the mapping  $u, p : (0, T) \rightarrow H_0^1(\Omega)$  satisfying a.e. in  $(0, T)$  and for each  $v, q \in H_0^1(\Omega)$  the equalities

$$(2.3) \quad \begin{aligned} \frac{d}{dt}(u - L\chi(p), v) + (\nabla u, \nabla v) &= 0, \\ u(0) &= u_0, \end{aligned}$$

$$(2.4) \quad \begin{aligned} \xi^2 \frac{d}{dt}(p, q) + \xi^2(T^0(\nabla p), \nabla q) &= (f_0(p), q) + \xi^2(F(u)\Phi^0(\nabla p), q), \\ p(0) &= p_0, \end{aligned}$$

Consider a strongly monotone operator  $T^0$  (strictly convex anisotropy). We then have a basic theorem (see [9]):

**Theorem 2.1.** *If  $u_0, p_0 \in H_0^1(\Omega)$  and  $\xi$  remains fixed, then there is a unique solution  $u^\xi, p^\xi \in L_2(0, T; H_0^1(\Omega))$  of the weak problem (2.3)–(2.4), for which*

$$\frac{\partial u^\xi}{\partial t}, \frac{\partial p^\xi}{\partial t} \in L_2(0, T; L_2(\Omega)).$$

The matched asymptotics as used e.g. in [6] gives the recovery of the Stefan condition and the Gibbs-Thomson law at the phase interface (see also [9]):

**Theorem 2.2.** *On the manifold  $\Gamma_0$ , the Stefan condition for the absolute terms in the outer expansion of temperature holds:*

$$|\nabla r|^2 \left( \frac{\partial u_0}{\partial r} \Big|_s - \frac{\partial u_0}{\partial r} \Big|_l \right) = Lv_{\Gamma, \Phi, 0},$$

and the Gibbs-Thomson law for the absolute term in the inner expansion of the phase function holds:

$$\int_{\mathbb{R}} \left( -\kappa_{\Gamma, \Phi, 0} \frac{\partial \bar{p}_0}{\partial z} - F(\bar{u}_0) \left| \frac{\partial \bar{p}_0}{\partial z} \right| - \frac{\partial \bar{p}_0}{\partial z} v_{\Gamma, \Phi, 0} \right) \frac{\partial \bar{p}_0}{\partial z} dz = 0.$$

**Remark.** Concerning the statement of Theorem 2.2, the solution and other quantities of (1.1) are formally expanded into the series in powers of  $\xi$  far from  $\Gamma^h$ :

$$u(t, x; \xi) = u_0(t, x) + u_1(t, x)\xi + u_2(t, x)\xi^2 + \mathcal{O}(\xi^3),$$

$$p(t, x; \xi) = p_0(t, x) + p_1(t, x)\xi + p_2(t, x)\xi^2 + \mathcal{O}(\xi^3),$$

and near  $\Gamma^h$  with the change to radial-tangential coordinates  $r, s$  and stretching  $r = \xi z$

$$\bar{u}(z, s, t; \xi) = \bar{u}_0(z, s, t) + \bar{u}_1(z, s, t)\xi + \bar{u}_2(z, s, t)\xi^2 + \mathcal{O}(\xi^3),$$

$$\bar{p}(z, s, t; \xi) = \bar{p}_0(z, s, t) + \bar{p}_1(z, s, t)\xi + \bar{p}_2(z, s, t)\xi^2 + \mathcal{O}(\xi^3).$$

### 3. NUMERICAL SCHEME

We solve the equations (1.1) numerically by means of the tools used in [11], [6]. For this purpose, we set  $\Omega = (0, L_1) \times (0, L_2)$ , denote  $\mathcal{H}_h$  the space of grid functions and denote

$$\begin{aligned}
 h_1 &= \frac{L_1}{N_1}, & h_2 &= \frac{L_2}{N_2}, \\
 \omega_h &= \{[ih_1, jh_2] \mid i = 1, \dots, N_1 - 1; j = 1, \dots, N_2 - 1\}, \\
 \bar{\omega}_h &= \{[ih_1, jh_2] \mid i = 0, \dots, N_1; j = 0, \dots, N_2\}, \\
 \mathbf{x}_{ij} &= [x_{ij}^1, x_{ij}^2], & u_{ij} &= u(\mathbf{x}_{ij}), \\
 u_{\bar{x}_1, ij} &= \frac{u_{ij} - u_{i-1, j}}{h_1}, & u_{x_1, ij} &= \frac{u_{i+1, j} - u_{ij}}{h_1}, \\
 u_{\bar{x}_2, ij} &= \frac{u_{ij} - u_{i, j-1}}{h_2}, & u_{x_2, ij} &= \frac{u_{i, j+1} - u_{ij}}{h_2}, \\
 u_{\bar{x}_1 x_1, ij} &= \frac{1}{h_1^2} (u_{i+1, j} - 2u_{ij} + u_{i-1, j}),
 \end{aligned}$$

and

$$\bar{\nabla}_h u = [u_{\bar{x}_1}, u_{\bar{x}_2}], \quad \nabla_h u = [u_{x_1}, u_{x_2}], \quad \Delta_h u = u_{\bar{x}_1 x_1} + u_{\bar{x}_2 x_2}.$$

We propose a semi-discrete scheme for the problem (1.1) based on spatial discretisation by finite differences as follows

$$\begin{aligned}
 (3.1) \quad & \dot{u}^h = \Delta_h u^h + L\chi'(p^h)\dot{p}^h, \\
 & u^h|_{\gamma_h} = 0, \quad u^h(0) = \mathcal{P}_h u_0, \\
 (3.2) \quad & \xi^2 \dot{p}^h = \xi^2 \nabla_h \cdot T^0(\bar{\nabla}_h p^h) + f_0(p^h) + \xi^2 \Phi^0(\bar{\nabla}_h p^h) F(u^h) \text{ on } \omega_h, \\
 & p^h|_{\gamma_h} = 0, \quad p^h(0) = \mathcal{P}_h p_0,
 \end{aligned}$$

where the solution is a map  $u^h, p^h : < 0, T > \rightarrow \mathcal{H}_h$ ,  $\mathcal{P}_h$  restricts the initial condition  $u_0$  and  $p_0$  on the grid  $\bar{\omega}_h$ . As in [6], [8] and related work, the semi-discrete scheme is solved by the Mersn variant of the 4-th order Runge-Kutta method. We mention, that the scheme (3.1)–(3.2) is convergent (see [9]).

**Theorem 3.1.** *If  $u_{\text{ini}}, p_{\text{ini}} \in H^2(\Omega) \cap H_0^1(\Omega)$ , then the solution of the semi-discrete scheme (3.1)–(3.2) for the method of lines converges in  $L_2(0, T; L_2(\Omega))$  to the weak solution of (2.3)–(2.4).*

#### 4. COMPUTATIONAL RESULTS

We have performed a series of computations by using (3.1)–(3.2) to show that it yields a good approximation of the original problem and to investigate the solution itself. In this text, we show the quantitative solution analysis for the dendritic growth. We measure the difference between two computations by means of the following norms:

$$\begin{aligned}
 \text{Error}_{L_\infty-L_2} &= \max_{k=0, \dots, N_T} \left( \int_{\Omega} |\mathcal{I}_h u^h(k\Delta t) - \mathcal{I}_{\tilde{h}} \tilde{u}^{\tilde{h}}(k\Delta t)|^2 dx \right)^{\frac{1}{2}}, \\
 \text{Error}_{L_\infty-L_\infty} &= \max_{k=0, \dots, N_T} \max_{x \in \Omega} |\mathcal{I}_h u^h(k\Delta t) - \mathcal{I}_{\tilde{h}} \tilde{u}^{\tilde{h}}(k\Delta t)|, \\
 \text{Error}_{L_\infty-\mathcal{H}} &= \max_{k=0, \dots, N_T} \varrho^*(\Gamma^h(k\Delta t), \Gamma^{\tilde{h}}(k\Delta t)),
 \end{aligned}$$

where  $\mathcal{I}_h$  is the piece-wise linear interpolation operator,  $k$  is the index of the output time slice considered in this measurement varying from 0 to  $N_T$ ,  $\varrho^*$  the Hausdorff distance between compact sets. The level set is

$$\Gamma^h(t) = \left\{ x \in \Omega \mid \mathcal{I}_h(p^h(t))(x) = \frac{1}{2} \right\}.$$

We evaluate the experimental orders of convergence defined as follows

$$\frac{\text{Error}_h}{\text{Error}_{\tilde{h}}} = \left( \frac{h + \xi}{\tilde{h} + \tilde{\xi}} \right)^{EOC_h}, \quad \frac{\text{Error}_{DoF}}{\text{Error}_{\widetilde{DoF}}} = \left( \frac{DoF}{\widetilde{DoF}} \right)^{EOC_{DoF}}.$$

We set  $F(u) = \beta(u - 1)$ ,  $\beta > 0$  with a suitable cut-off,  $r_{\text{crit}}$  is the diameter of the initial crystallization seed. In the computations, the parameter  $\Delta t$  means the period of the data output,  $N_T$  number of such outputs,  $N_\tau$  total number of time steps performed by the adaptive time solver,  $tol$  tolerance for the adaptive Mersn time stepping (see also [18]) and  $DoF$  total number of degrees of freedom,  $DoF = N_\tau \times (N_1 - 1) \times (N_2 - 1)$ .

**Example 1.** It shows the growing dendrite with imposed weak (convex) anisotropy. We compare the solution on four grids with the solution on a very fine mesh by measuring their difference. The problem setting and the finest-grid parameters are indicated in Table 4.1. The shape of the solution is presented in Figure 4.1, the level-set dynamics in Figure 4.2. The measured differences are summarized in Table 4.2 and the EOC's in Tables 4.3 and 4.4. The CPU time is given by the system used in this case (LINUX RedHat 8.0 on the Pentium IV, 2.66 GHz, 1GB RAM, the code compiled by the Intel Fortran Compiler 8.0).

$L$	$\beta$	$m$	$A$	$\xi$	$\Omega$	$r_{\text{crit}}$	$\Theta_0$
1.0	200.0	4	0.06300	0.00400	$(0.3) \times (0.3)$	0.05	1.0000
$\Delta t$	$N_T$	$N_\tau$	$tol$	mesh	DoF	CPU	
0.015	10	33226	0.001	0.00375	242423023252	708520.60	

**Table 4.1.** Table of the finest experiment parameters for Example 1.

Mesh $h$	$\xi$	$N_T$	DoF	$L_\infty - L_2$ error of $u$	$L_\infty - L_\infty$ error of $u$	$L_\infty - \mathcal{H}$ error of $\Gamma^h$	CPU
0.0075000	0.0080	8819	2807987238	0.1562571	0.3834383	0.0956174	45461.60
0.0060000	0.0070	13287	6616952574	0.1185770	0.3230643	0.0715796	106320.00
0.0050000	0.0060	18734	13443555868	0.0789952	0.2471442	0.0470672	220544.09
0.0042857	0.0050	25320	24742754640	0.0393572	0.1460856	0.0231805	407235.59

**Table 4.2.** Table of numerical parameters and convergence errors for Example 1.

Mesh $h$	$\xi$	$N_T$	DoF	$EOC_h$ for $L_\infty - L_2$ of $u$	$EOC_h$ for $L_\infty - L_\infty$ of $u$	$EOC_h$ for level sets
0.0075000	0.0080	10	2807987238	0.0000000	0.0000000	0.0000000
0.0060000	0.0070	10	6616952574	1.5688162	0.9740567	1.6461653
0.0050000	0.0060	10	13443555868	2.4313986	1.6035485	2.5095652
0.0042857	0.0050	10	24742754640	4.1123587	3.1034392	4.1805747

**Table 4.3.** Table of  $EOC_h$  coefficients (*Error* versus  $h + \xi$ ) for Example 1.

Mesh $h$	$\xi$	$N_T$	DoF	$EOC_{DoF}$ for $L_\infty - L_2$ of $u$	$EOC_{DoF}$ for $L_\infty - L_\infty$ of $u$	$EOC_{DoF}$ for level sets
0.0075000	0.0080	10	2807987238	0.0000000	0.0000000	0.0000000
0.0060000	0.0070	10	6616952574	0.3219211	0.1998764	0.3377931
0.0050000	0.0060	10	13443555868	0.5729937	0.3778990	0.5914148
0.0042857	0.0050	10	24742754640	1.1420833	0.8618864	1.1610282

**Table 4.4.** Table of  $EOC_{DoF}$  coefficients (*Error* versus  $DoF$ ) for Example 1.

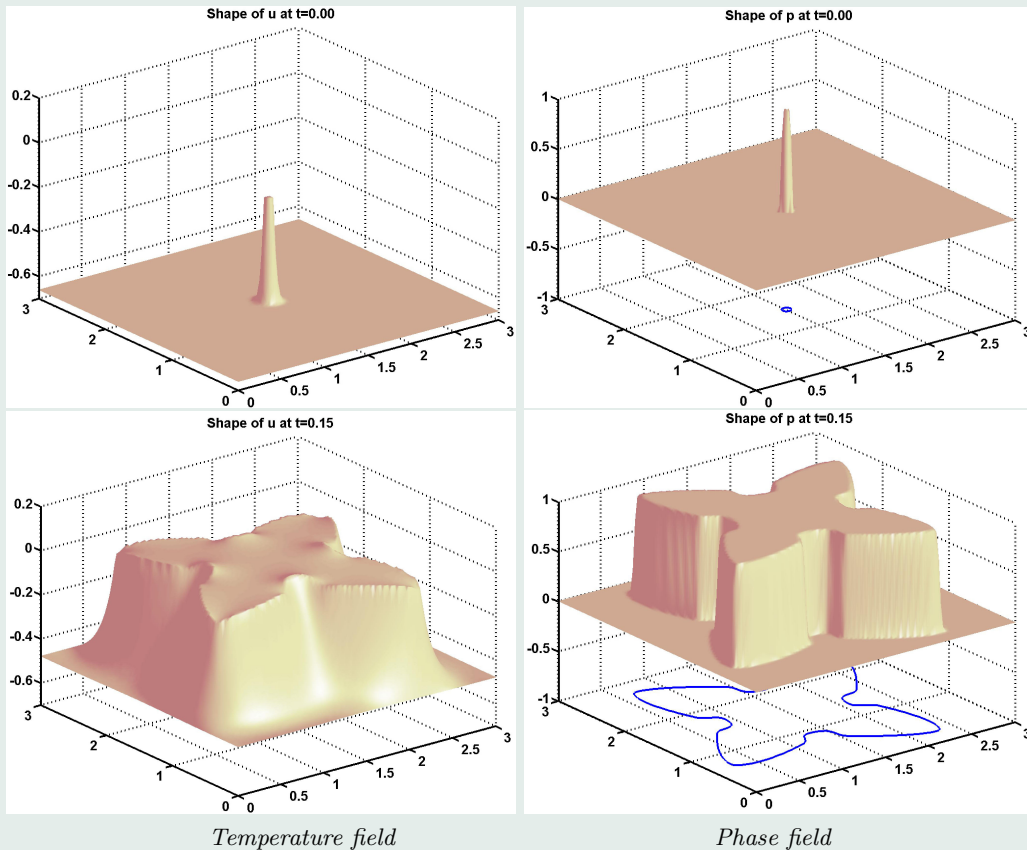
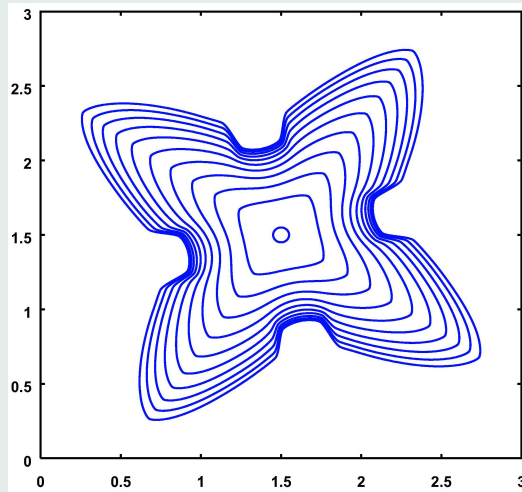


Figure 4.1. Shape of the solution for Example 1.



**Figure 4.2.** Evolution of the level set  $\frac{1}{2}$  for Example 1.

**Example 2.** It shows the growing dendrite with imposed stronger (non-convex) anisotropy. We compare the solution on four grids with the solution on a very fine mesh by measuring their difference. The problem setting and the finest-grid parameters are indicated in Table 4.5. The shape of the solution is presented in Figure 4.3, the level-set dynamics in Figure 4.4. The measured differences are summarized in Table 4.6 and the EOC's in Tables 4.7 and 4.8. The CPU time is given by the system used in this case (HP-UX 11.0 on the PARISC system B2000, 700 MHz, 256 MB RAM, the code compiled by the HP Fortran Compiler.)

$L$	$\beta$	$m$	$A$	$\xi$	$\Omega$	$r_{\text{crit}}$	$\Theta_0$
1.0	200.0	4	0.09000	0.00400	$(0.3) \times (0.3)$	0.05	-1.0000

$\Delta t$	$N_T$	$N_\tau$	$tol$	mesh	DoF	CPU
0.015	10	36230	0.001	0.00375	46258536460	1474862.00

**Table 4.5.** Table of the finest experiment parameters for Example 2.

Mesh $h$	$\xi$	$N_T$	DoF	$L_\infty - L_2$ error of $u$	$L_\infty - L_\infty$ error of $u$	$L_\infty - \mathcal{H}$ error of $\Gamma^h$	CPU
0.0075000	0.0080	10	3008580498	0.1591132	0.4058937	0.0949960	65341.21
0.0060000	0.0070	10	7129396632	0.1227783	0.3541477	0.0727318	163706.90
0.0050000	0.0060	10	14587413456	0.0832208	0.2759567	0.0484809	349094.09
0.0042857	0.0050	10	26962957584	0.0421468	0.1717665	0.0244523	689769.00

**Table 4.6.** Table of numerical parameters and convergence errors for Example 2.

Mesh $h$	$\xi$	$N_T$	DoF	$EOC_h$ for $L_\infty - L_2$ of $u$	$EOC_h$ for $L_\infty - L_\infty$ of $u$	$EOC_h$ for level sets
0.0075000	0.0080	10	3008580498	0.0000000	0.0000000	0.0000000
0.0060000	0.0070	10	7129396632	1.4738454	0.7753530	1.5183069
0.0050000	0.0060	10	14587413456	2.3278870	1.4933487	2.4280040
0.0042857	0.0050	10	26962957584	4.0157305	2.7984488	4.0399686

**Table 4.7.** Table of  $EOC_h$  coefficients (*Error* versus  $h + \xi$ ) for Example 2.

Mesh $h$	$\xi$	$N_T$	DoF	$EOC_{DoF}$ for $L_\infty - L_2$ of $u$	$EOC_{DoF}$ for $L_\infty - L_\infty$ of $u$	$EOC_{DoF}$ for level sets
0.0075000	0.0080	10	3008580498	0.0000000	0.0000000	0.0000000
0.0060000	0.0070	10	7129396632	0.3004731	0.1580713	0.3095375
0.0050000	0.0060	10	14587413456	0.5431841	0.3484547	0.5665451
0.0042857	0.0050	10	26962957584	1.1074919	0.7717797	1.1141765

**Table 4.8.** Table of  $EOC_{DoF}$  coefficients (*Error* versus  $DoF$ ) for Example 2.

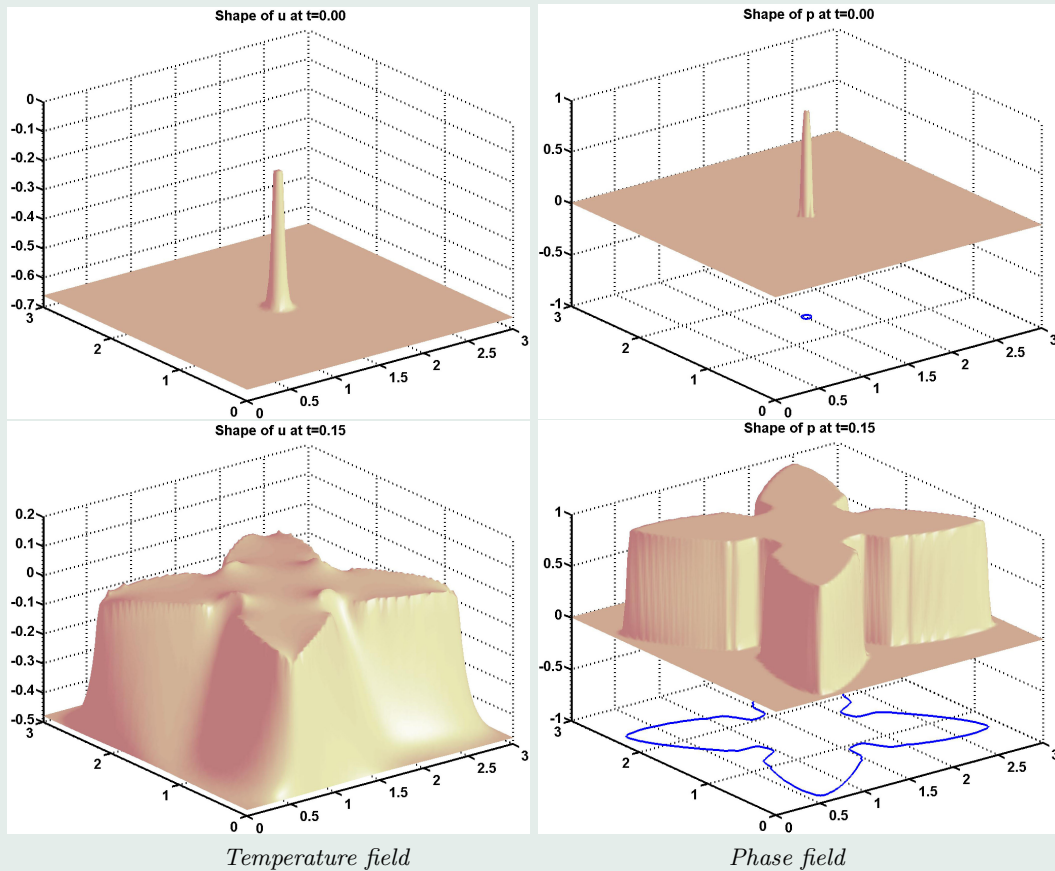


**Figure 4.3.** Shape of the solution for Example 2.

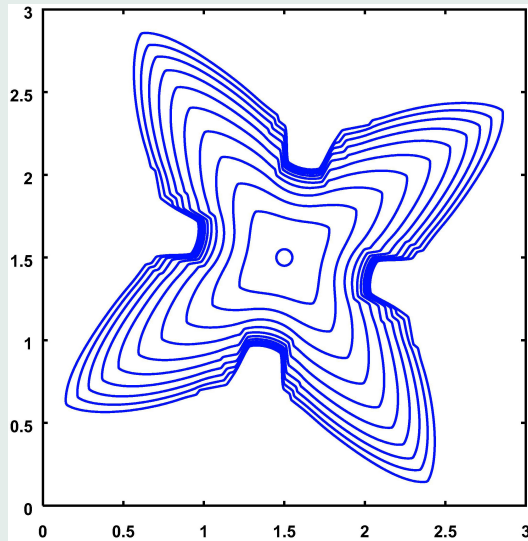


**Figure 4.4.** Evolution of the level set  $\frac{1}{2}$  for Example 2.

**Acknowledgement.** This work was partly supported by the research plan No. MSM 6840770010 *Applied Mathematics in Technical and Physical Sciences* and by the project No. LC06052 “*Nečas Center for Mathematical Modelling*” of the Ministry of Education, Youth and Sport of the Czech Republic..

1. Alikakos N. D. and Bates P. W., *On the singular limit in a phase field model of phase transitions*. Ann. Inst. Henri Poincaré, **5** (1988), 141–178.
2. Beneš M., *Modelling of dendritic growth in pure substances*. Acta Techn. CSAV, **39** (1994), 375–397.
3. ———, *On a computational comparison of phase-field and sharp-interface model of microstructure growth in solidification*. Acta Techn. CSAV, **41** (1996), 597–608.
4. ———, *Anisotropic phase-field model with focused latent-heat release*. FREE BOUNDARY PROBLEMS: Theory and Applications II, GAKUTO International Series Mathematical Sciences and Applications, **14** 18–30, Chiba, Japan, 2000.
5. ———, *Numerical solution of phase-field equations with a gradient coupling term*. In W. Jäger, J. Nečas, O. John, K. Najzar, and J. Stará, editors, Partial Differential Equations – Theory and Numerical Solution, 25–33, New York, 2000.
6. ———, *Mathematical analysis of phase-field equations with numerically efficient coupling terms*. Interfaces and Free Boundaries **3** (2001), 201–221.
7. ———, *Mathematical and computational aspects of solidification of pure substances*. Acta Mathematica Universitatis Comenianae, **70(1)** (2001), 123–152.
8. ———, *Diffuse-interface treatment of the anisotropic mean-curvature flow*. Applications of Mathematics, **48(6)** (2003), 437–453.
9. ———, *Diffuse interface model of microstructure formation in solidification with anisotropy*. In preparation, 2006.
10. Beneš M., Hilhorst D., and Weidenfeld R., *Interface dynamics of an anisotropic Allen-Cahn equation*. In Nonlocal elliptic and parabolic problems, Institute of Mathematics, Polish Academy of Sciences, **66**, pp. 39–45 eds. P. Biler, G. Karch and T. Nadzieja, ISSN 0137-6934, Warsaw, 2004.
11. Beneš M. and Mikula K., *Simulation of anisotropic motion by mean curvature–comparison of phase-field and sharp-interface approaches*. Acta Math. Univ. Comenianae, **67(1)** (1998), 17–42.
12. Blowey J. F. and Elliott C. M., *Curvature dependent phase boundary motion and parabolic obstacle problems*. In Ni W., Peletier L., and Vasquez J. L., editors, Proc. IMA Workshop on Degenerate Diffusion, pp. 19–60, New York, 1993.
13. Caginalp G., *An analysis of a phase field model of a free boundary*. Arch. Rational Mech. Anal., **92** (1986), 205–245.
14. Caginalp G. and Fife P. C., *Dynamics of layered interfaces arising from phase boundaries*. SIAM J. Appl. Math., **48** (1988), 506–518.
15. Elliott C. M. and Gardiner A. R., *Double-obstacle phase-field computations of dendritic growth*. Technical report, CMAIA, University of Sussex, Brighton, 1996. Report No. 96/19.
16. Elliott C. M., Paolini M., and Schätzle R., *Interface estimates for the fully anisotropic Allen-Cahn equation and anisotropic mean curvature flow*. Math. Models Methods Appl. Sci., **6** (1996), 1103–1118.

17. Gurtin M., *Thermomechanics of Evolving Phase Boundaries in the Plane*. Clarendon Press, Oxford, 1993.
18. Holodniok M., Klíč A., Kubíček M., and Marek M., *Methods of Analysis of Nonlinear Dynamical Models*. Academia, Prague, 1984.
19. Kessler D. A., Koplik J., and Levine H., *Geometrical models of interface evolution. III. theory of dendritic growth*. Phys. Rev. A, **31** (1985), 1712–1717.
20. Luckhaus S. and Modica L., *The Gibbs-Thompson relation within the gradient theory of phase transitions*. Arch. Rational Mech. Anal., bf 107 (1989), 71–83.
21. Ohta T., Mimura M. and Kobayashi R., *Higher-dimensional localized patterns in excitable media*. Physica D, **34** (1989), 115–144.
22. Visintin.A. *Models of Phase Transitions*. Birkhäuser, Boston, 1996.
23. Warren J. A. and Langer J. S., *Prediction of dendritic spacings in a directional-solidification experiment*. Phys. Rev. E, **47** (1993), 2702–2712.
24. Wheeler A. A. and McFadden G. B., *On the notion of a  $\xi$  vector and a stress tensor for a general class of anisotropic diffuse interface models*. Proc. R. Soc. Lond. **A** (1997), 1611–1630.

Michal Beneš, Department of Mathematics, Faculty of Nuclear Sciences and Physical Engineering, Czech Technical University in Prague and Institute of Thermomechanics, Academy of Sciences of Czech Republic, *e-mail*: [benes@km1.fjfi.cvut.cz](mailto:benes@km1.fjfi.cvut.cz)